Int. J. Electrochem. Sci., 15 **(2020)** 4684 – 4701, doi: 10.20964/2020.05.83

International Journal of ELECTROCHEMICAL SCIENCE
www.electrochemsci.org

An Ionic Liquid-Present Method for Preparing Micro-sized Octahedral Particles of Co_3O_4 and Their Applications as Anode Materials for Lithium Ion Batteries

Keqiang Ding[1,2,3], Xiaojing Gao[1], Jingwei Han[1], Xiangming He[2], Runling Qu[1], Lanjun Zhou[1], Hongmin Dou[3], Hui Wang[3], Li Wang[2,*]*

[1] National Demonstration Center for Experimental Chemistry Education, Hebei Key Laboratory of Organic Functional Molecules, Hebei Key Laboratory of Inorganic Nanomaterials, College of Chemistry and Material Science, Hebei Normal University, Shijiazhuang, Hebei 050024, China
[2] Institute of Nuclear & New Energy Technology, Tsinghua University, Beijing 100084, China
[3] Hebei LingDian New Energy Technology Co., Ltd, Tangshan, Hebei, 064200, China
[*]E-mail: dkeqiang@263.net, wang-l@tsinghua.edu.cn

Received: 12 January 2020 / *Accepted:* 24 February 2020 / *Published:* 10 April 2020

For the first time, tricobalt tetraoxide (Co_3O_4) particles with a well-defined octahedral structure and a size more than 8 μm were prepared via an ionic liquid-present dissolving-drying-calcination method using cobaltous acetate tetrahydrate ($Co(CH_3COO)_2 \cdot 4H_2O$) as the precursor in this work. Different from the previous works, a kind of ionic liquids (ILs) was employed as one main component of the preparation solution. The materials prepared in the presence of 1-butyl-3-methylimidazolium bromide, 1-butyl-3-methylimidazolium tetrafluoroborate and 1-butyl-3-methylimidazolium chloride were respectively nominated as material a, b and c. As indicated by the XRD and XPS analysis, CoO and Co_3O_4 were the major components of material a and b, and Co_3O_4 was the main substance of material c. As confirmed by the obtained SEM images, octahedral particles of Co_3O_4 with a size greater than 8 μm were prepared in material c. When being used as anode materials for lithium ion batteries (LIBs), material a, b and c at the current density of 100 mA g^{-1} exhibited an initial discharge capacity of 600, 612 and 878 mAh g^{-1}, respectively. Particularly, material c was able to deliver a discharge capacity of 336 mAh g^{-1} after 10 cycles even under the current density of 500 mA g^{-1}. A fact that octahedral particles of Co_3O_4 with a size more than 8 μm could be prepared using an ionic liquid-present method was presented in this work, which was very beneficial to the development of metal oxides based anode materials of LIBs as well as the exploration of micro-devices.

Keywords: cobaltous acetate tetrahydrate; ionic liquid; micron-sized octahedron Co_3O_4 particles; anode materials; lithium ion batteries.

1. INTRODUCTION

Nowadays, the issue of global warming has become a tricky problem [1] which is generally thought to be mainly from the large scale emission of CO_2. And, it has reached a consensus that the fuel vehicle exhaust is the main source of producing CO_2, thus, utilizing electric vehicle (EV) to replace fuel vehicle is considered to be the most practicable way to greatly reduce CO_2 emission amount while maintaining the continuous development of urban transportation. Therefore, battery, as the key part of an EV, becomes particularly crucial for the final commercialization of an EV [2]. Lithium ion batteries (LIBs) [3], due to its excellent electrochemical properties compared to the traditional batteries like lead acid battery, were selected as the most preferred kind of battery to power an EV. Of late, it is urgently claimed by LIBs-related researchers that the theoretical capacity (372 mAh g^{-1}) of graphite (one conventional LIBs anode material) is lower which has severely blocked the further development of high energy density LIBs. Hence, many novel kinds of LIBs anode materials have been eagerly developed in order to substitute graphite. For all we know, some elementary metals such as Sn [4], several kinds of carbon [5-7] and a large number of transition metal oxides (TMOs) [8] have been explored as the major three types of LIBs anode materials in recent years. Among the TMOs, tricobalt tetraoxide (Co_3O_4) was thought as one of the most promising TMOs to replace the current anode material of graphite owing to its higher theoretical capacity (890 mAh g^{-1}) and higher discharge terrace (1.0 V versus Li^+/Li) [9]. Nevertheless, the volume variation during the charge and discharge process as well as the rather lower electrical conductivity severely restricted the practical application of Co_3O_4 as anode materials of LIBs. Consequently, particles of Co_3O_4 with various morphologies and sizes have been prepared desiring to promote the electrochemical performance of Co_3O_4 while retaining its original superior properties. Although Co_3O_4 particles with morphologies like peony-like shape [10], porous nanosheet [11,12] and nanocubes [13] have been fabricated in the last several years, Co_3O_4 particles with an octahedron morphology still attracted more research interests mostly because of its superior electrochemical performances when employed as LIBs anode materials. Summarily, there are two conventional methods to produce Co_3O_4 octahedral particles, one way for preparing Co_3O_4 octahedron particles was realized through the direct decomposition of $Co(OH)_2$. For example, Li's group [14] announced that the shape of Co_3O_4 particles could be easily adjusted by varying the contents of both NaOH and $Co(NO_3)_2{\cdot}6H_2O$ in the absence of capping agents. The other way to prepare Co_3O_4 octahedral particles was achieved via the direct pyrolysis of metal-organic frameworks. For instance, Zheng's group [15] fabricated ultrafine Co_3O_4 nanoparticles via a pyrolysis process of metal-organic frameworks (MOFs) using cobalt nitrate hexahydrate and 2-methylimidazole as the initial materials. To be clear, in Li [14] and Zheng's work [15], all the heating treatments were conducted in an inert gas atmosphere rather than in an air condition. Very recently, a composite containing Co_3O_4 and nitrogen doped carbon was synthesized by Meng's group [16], in which 1-butyl-3-methylimidazolium dicyanamide and $Co(NO_3)_2{\cdot}6H_2O$ were employed as the precursors and the calcination process was accomplished at 700 ºC in an argon-filled tube furnace. To our knowledge, no paper announcing the synthesis of Co_3O_4 octahedral particles with a size greater than 8 μm in an air atmosphere was published so far, not to speak of the ILs-containing Co_3O_4 preparation system.

In this work, three kinds of ILs were respectively introduced into an ethanol-containing cobaltous

acetate solution, and after the drying and calcination process, cobalt oxides were easily produced. To our surprise, the particles prepared in the presence of 1-butyl-3-methylimidazolium chloride not only had a larger particle size (more than 8.0 μm) but also presented a well-defined octahedron morphology. Most interestingly, it was found that material c, which had the largest particle size among all prepared materials, exhibited the best electrochemical behavior among all prepared materials in terms of discharge capacity value, cycling stability and rate capability. At the current density of 100 mA g^{-1}, the initial discharge capacity of material c was 878 mAh g^{-1}, and even after 20 cycles, the discharge capacity was still maintained as high as 647 mAh g^{-1}. Showing the fact that the octahedron particles of Co_3O_4 with a size more than 8 μm as well as an acceptable electrochemical performance can be prepared simply via an ionic liquid-present dissolving-drying-calcination method was the main contribution of this work which have pioneered a new avenue for fabricating metal oxide based anode materials of LIBs, being of far-reaching significance to the further development of micro-devices.

2. EXPERIMENTAL

2.1. Materials

All the chemical reagents including acetate tetrahydrate were purchased from Macklin Co. Ltd. (Shanghai). In the battery performance test, all the materials and reagents such as electrolyte of 1 M $LiPF_6$, acetylene black, polyvinylidene fluoride and the coin cells were bought from Tianjin Liangnuo S&T Developing Co. Ltd. Ionic liquids employed in this research were purchased from Saideng Ionic Liquid Co. Ltd (Shenyang). All chemicals were used as received and not subjected to any further purification.

2.2. Preparation of Co_3O_4 octahedral particles

Figure 1. Photos of all materials appearing in the preparation process. Photo 1 was for cobaltous acetate tetrahydrate. Photo 2 was the photo of the suspension solution containing $Co(CH_3COO)_2 \cdot 4H_2O$, 1-butyl-3-methylimidazolium bromide, double-distilled water and ethanol. Photo 3 was the photo of the well-dried materials which was a black and viscous substance. Photo 4 was the final material, a black powder.

Firstly, 3 g of $Co(CH_3COO)_2 \cdot 4H_2O$ (photo 1 in Fig.1) and 0.75 g of 1-butyl-3-methylimidazolium bromide were thoroughly dissolved in a solution that consisted of 15 mL double-distilled water and 15 mL absolute ethanol. Secondly, the obtained solution was violently stirred for 15 min at room temperature producing a red-brown suspension solution (photo 2 in Fig.1). Subsequently, the resultant solution was placed in a well-sealed Teflon-lined autoclave and heated at 90 ºC for 15 h in a drying oven. And then, after being carefully filtered, and the obtained filter residue was continuously dried in air for 5 h to generate a black and viscous substance (photo 3 in Fig.1). Lastly, the black and viscous substances were calcined in a muffle furnace at 600 ºC for 2 h under an air atmosphere to harvest the final products (photo 4 in Fig.1). The materials prepared with ILs of 1-butyl-3-methylimidazolium bromide, 1-butyl-3-methylimidazolium tetrafluoroborate and 1-butyl-3-methylimidazolium chloride were called as material a, b and c, respectively.

2.3. Characterization

X-ray diffraction (Bruker AXS, D8 ADVANCE (Database version PDF-2004), Germany) was applied for analyzing the phase compositions of all the as-synthesized materials. The surface morphologies of all the as-prepared materials were seen by using scanning electron microscopy (HITACHI, SEM S-570). The elemental components of all the as-produced materials were probed by employing energy dispersive spectrometer (EDS, INCA Energy 350, England). Fourier transform infrared (FTIR) spectroscopy analysis was conducted on a Hitachi FT-IR 8900 spectrometer (Japan) with an intention to analyze the functional groups existing in the final materials. The valence states of the elements in all obtained materials were studied with the help of X-ray photoelectron spectroscopy (XPS, ESCALAB250Xi, ThermoFisher Scientific).

A CHI 660B electrochemical workstation (Shanghai Chenhua Apparatus, China) was employed to accomplish the cyclic voltammetry (CV) and electrochemical impedance spectroscopy (EIS) measurements. In the EIS test, the frequency scope of the alternating current (AC) was from 0.1 Hz to 100 kHz being along with a 5 mV amplitude.

The synthetic procedure of a working electrode has been well introduced in our previous work [17]. Briefly, the first step was to create a mixture that contained a type of material, acetylene black and polyvinylidene (The mass ratio of above three substances was 8:1:1). Secondly, a cream was produced through adding several drops of N-methyl pyrrolidone (NMP) into above resultant mixture. Subsequently, the obtained creams were spread on a well cleaned commercial Cu foil with the aid of a piece of glass. Lastly, the prepared cream-coated Cu foils were dried at 120 ºC in a vacuum oven for 6 h to generate the working electrode. Generally, the two-electrode cell (also called as a half-cell) was composed of a working electrode, 1 M $LiPF_6$, a separator of Celgard 2400 and a lithium metal foil. The assemblies of the two-electrode cell were conducted in a high pure nitrogen gas-filled glove box (ZKX, Nanjing NANDA instrument factory, China). The solvent, used to form 1M $LiPF_6$, was a mixed solvent that mainly consisted of dimethyl carbonate (DMC), ethylene carbonate (EC), ethyl methyl carbonate (EMC) and vinylene carbonate (VC). In the two-electrode cell, the metallic lithium foil was employed as both the counter and reference electrode. The galvanostatic charge-discharge testing was carried out

on an equipment of CT-3008W-5V20mA-S4 (Shenzhen Neware Electronics Co., Ltd. China). The cut-off potentials in the discharge and charge measurement were 0.01V to 3 V, respectively. The current densities in the cycling tests were 100, 300 and 500 mA g^{-1}, respectively.

3. RESULTS AND DISCUSSION

3.1 XRD and SEM characterization

XRD patterns for all prepared materials, as well as the standard XRD patterns of CoO and Co_3O_4, are illustrated in Fig.2a. The main diffraction peaks of at 31.3º ,37.0º , 44.9º, 59.6º and 65.5º matched well, respectively, with the (220), (311), (400), (511) and (440) plane of the standard XRD pattern of Co_3O_4, confirming the preparation of Co_3O_4 (JCPDS, Card No. 03-065-3103) in all synthesized materials [18]. Also, the characteristic diffraction peaks indexed to CoO [19], i.e., the diffraction peaks of appearing at 36.9 º (111), 42.6º (200) and 61.7º (220), were also visible particularly in pattern a and b, assuring that CoO as the other component was produced in all synthesized materials. No other diffraction peaks were exhibited suggesting that CoO and Co_3O_4 were the main components of all prepared materials. Additionally, the diffraction peaks assigned to carbon were not observed in Fig 2a, implying that the content of carbon in all prepared materials was low or the prepared carbon material was amorphous in nature [20]. The highest diffraction peaks were exhibited by material c which effectively documented that the crystallinity of material c was higher when compared to other two materials [20].

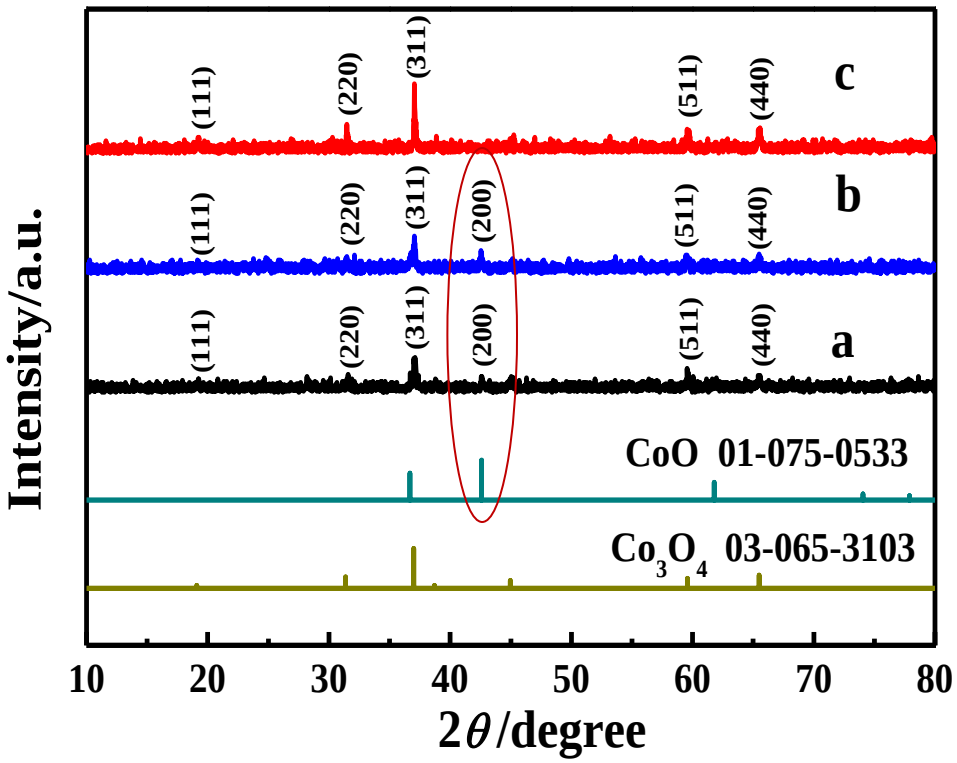

Figure 2a. XRD patterns of all as-synthesized materials including the standard patterns of Co_3O_4 and CoO. Pattern a, b and c corresponded to material a, b and c.

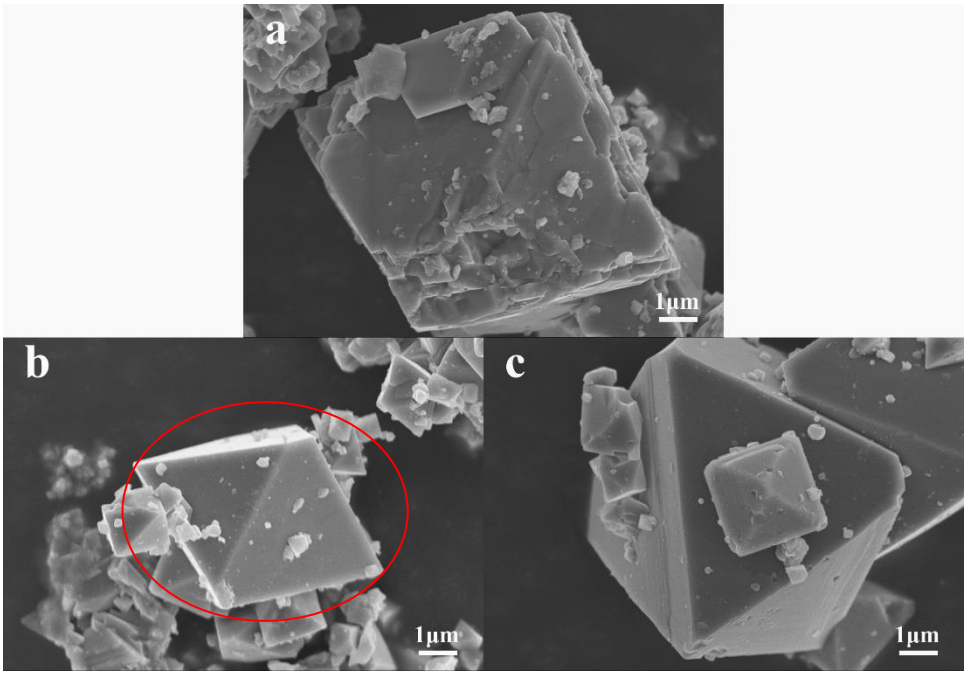

Figure 2b. SEM images of all as-prepared materials. Image a, b and c corresponded to material a, b and c.

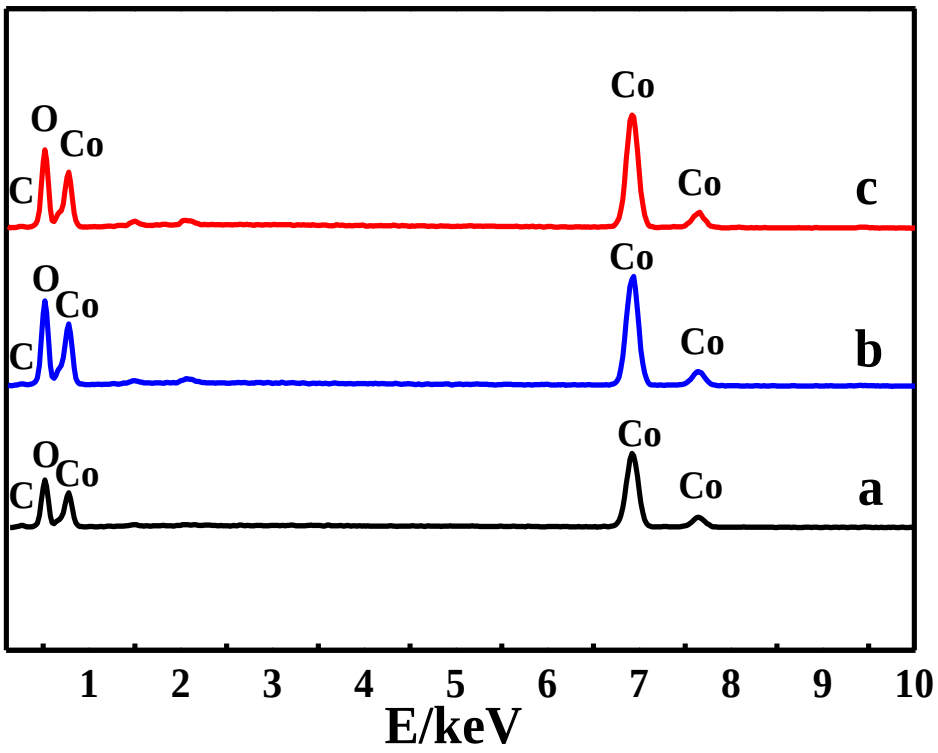

Figure 2c. EDS patterns for all prepared materials. Pattern a, b and c corresponded to material a, b and c.

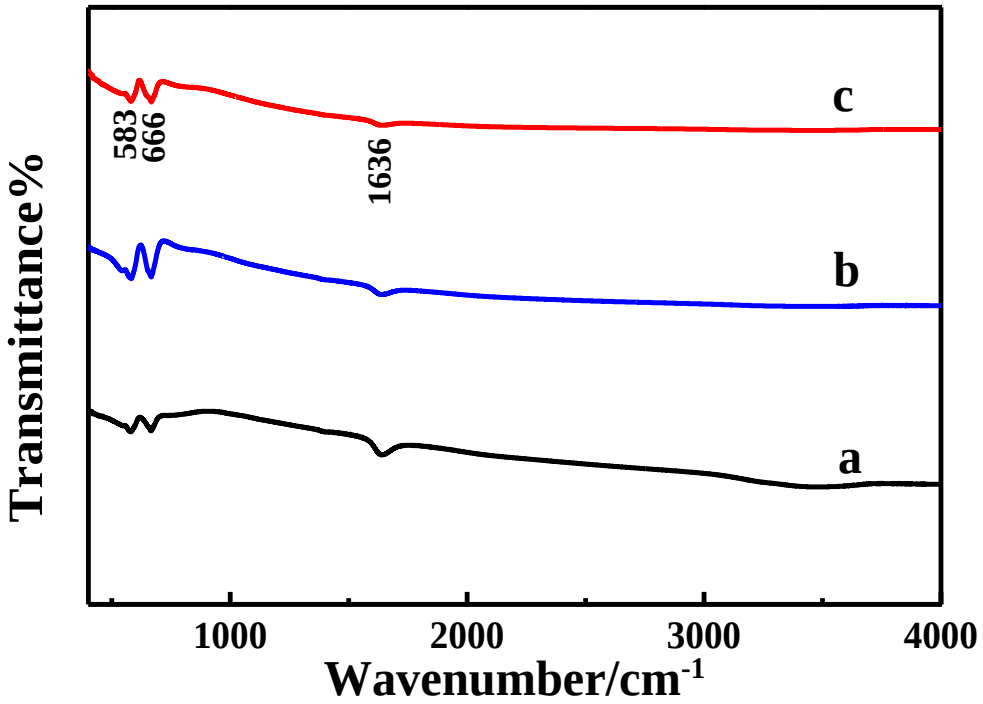

Figure 2d. FTIR spectra for all resultant materials. Curve a, b and c corresponded to material a, b and c.

SEM images with a scale of 1 μm for all synthesized materials are given in Fig.2b. For material a, except for some small irregular particles, a damaged particle with a size more than 7.3 μm was observed distinctly. In the case of material b, as red circled part, an octahedral particle with an edge of 4.6 μm was seen clearly, and some octahedral particles with a size close to 1 μm were also observed in material b. As for material c, a huge particle with a well-defined octahedron structure (whose edge length was close to 8.3 μm) was clearly presented. According to the XRD (Fig.2a) and XPS analysis (Fig.3b), the octahedron particles shown in Fig.2b should be Co_3O_4 particles. Co_3O_4 octahedron particles with various sizes have been fabricated in the erstwhile works. For instance, the size of the Co_3O_4 particles with a truncated octahedral morphology, which were prepared by Li's team using NaOH and $Co(NO_3)_2 \cdot 6H_2O$ as the starting materials, was about 600 nm [14]. The diameter of the Co_3O_4 nano-octahedra particles prepared by Sun's group [21] using $CoCl_2$, PVP and glucose as the precursors was about 387 nm. To our knowledge, this is the first time to report the synthesis of well-defined octahedron particles of Co_3O_4 with a size greater than 8 μm.

3.2 Chemical composition characterization

In the EDS patterns (Fig.2c), the peaks indexed to C, O and Co elements were displayed in all produced materials, implying that no other elements were remained in the final products. Here, the residual carbon was probably originated from the decomposition of ILs employed [16]. The atomic percentage of carbon in material a, b and c was, respectively, roughly measured to be 10.81%, 4.96% and 4.91%**.** The presence of a certain content of carbon in an electrode material was helpful to the electrochemical performance improvement of an electrode because of carbon's higher electronic

conductivity [22, 23]. The atomic yields of Co were approximately detected to be 37.67%, 37.41% and 39.85% in material a, b and c, respectively, indicating that more amounts of cobalt oxides were produced in material c, which was advantageous to the lithium storage improvement of a material since Co_3O_4 and CoO [24] were all anode materials of LIBs.

The FTIR curves of all synthesized materials (Fig.2d) revealed that for all the resultant materials, two absorption bands of at around 583 and 666 cm^{-1} were exhibited clearly which could be well ascribed to the cobalt-oxygen (Co-O) vibrational modes, further confirming the formation of Co_3O_4 [25] in all prepared materials. The absorption band positioned at 1636 cm^{-1} was, commonly, originated from the stretching and bending frequencies of adsorbed-water derived -OH group [25]. The weak and broad peak appearing at 3418 cm^{-1} was generally stemmed from the -OH group stretching mode of water [26]. Especially, no other absorption bands were found indicating that cobalt oxides were the main components of all produced materials, coinciding well with the XRD results (Fig.2a). The absence of other organic functional groups in the FTIR spectra of Fig.2d, also, suggested that most of carbon elements in all synthesized materials should exist in the form of carbon particles rather than organic molecules.

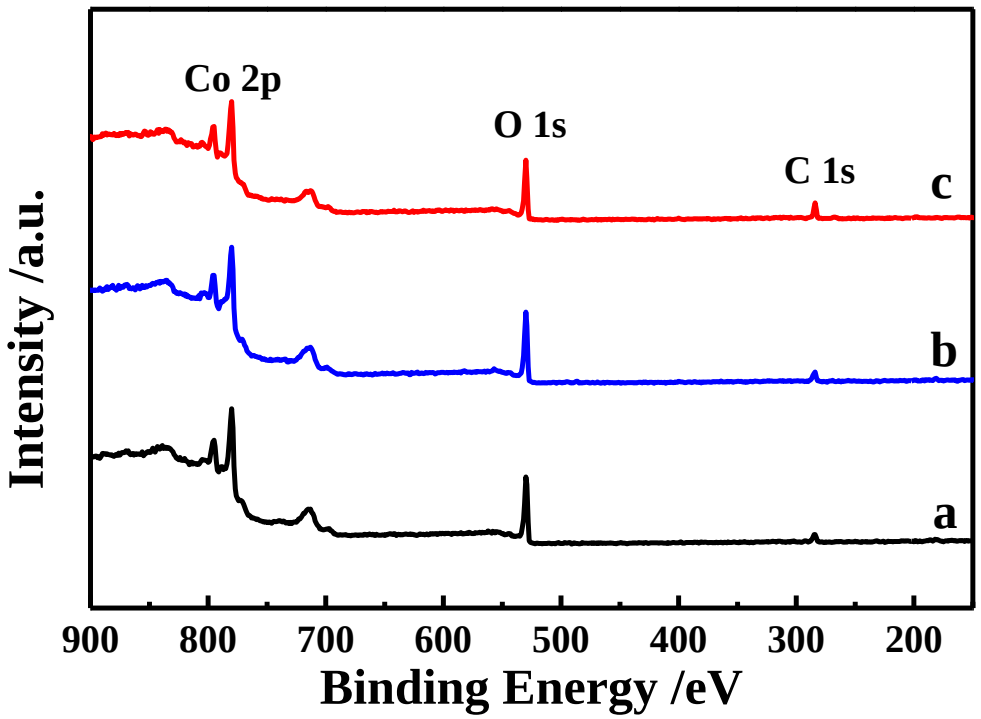

Figure 3a. Wide scan XPS survey spectra of all resultant materials. Pattern a, b and c corresponded to material a, b and c

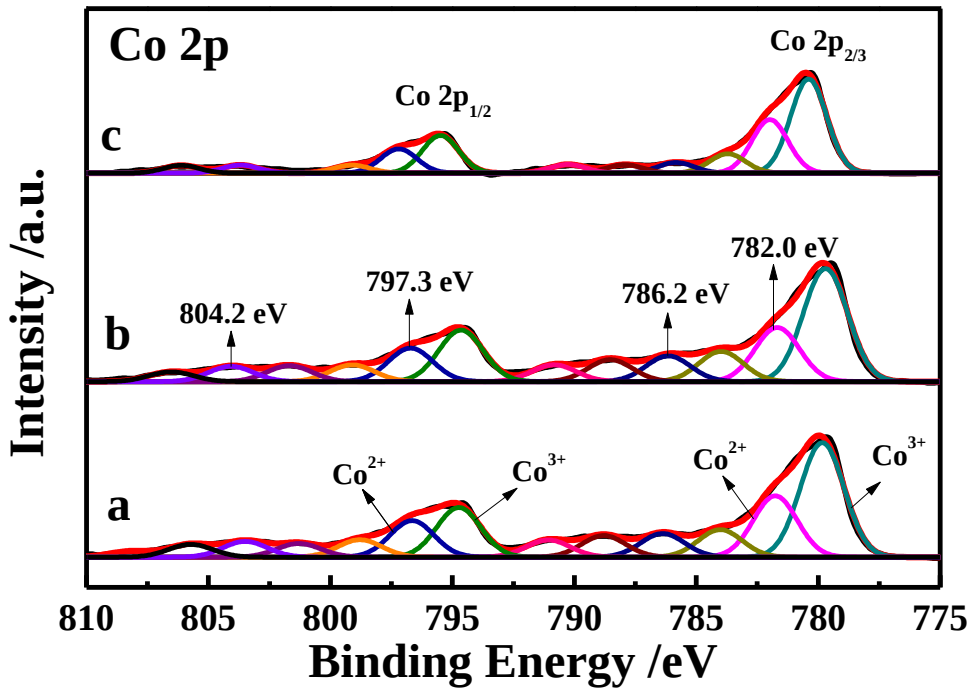

Figure 3b. Co2p spectrum of XPS spectra for all prepared materials. Curve a, b and c corresponded to material a, b and c.

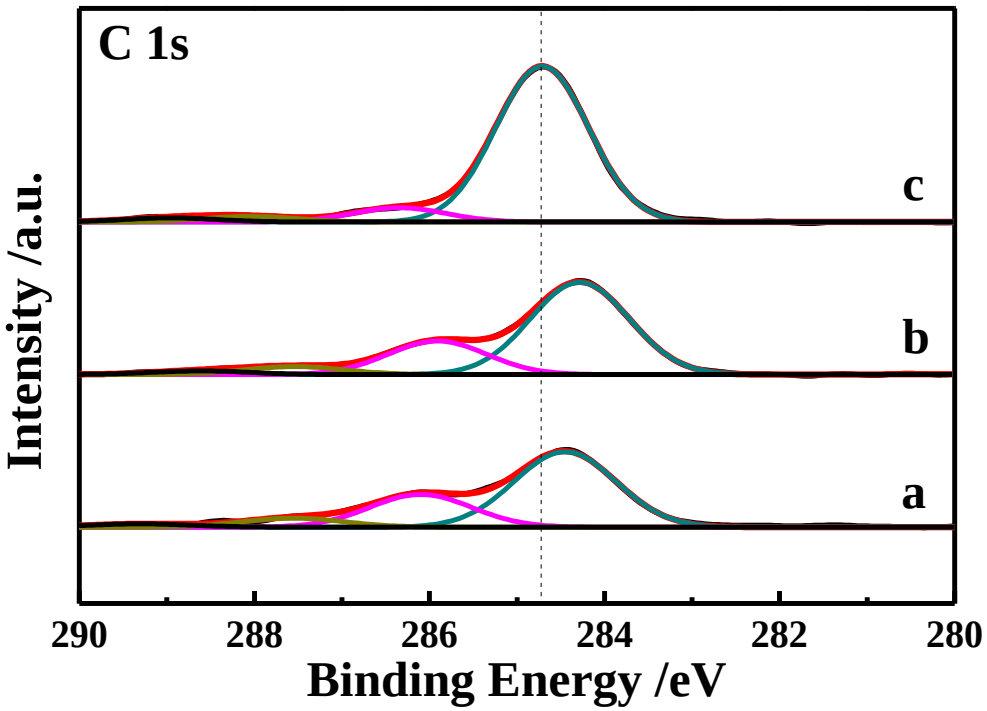

Figure 3c. O1s spectrum of XPS spectra for all synthesized materials. Curve a, b and c corresponded to material a, b and c.

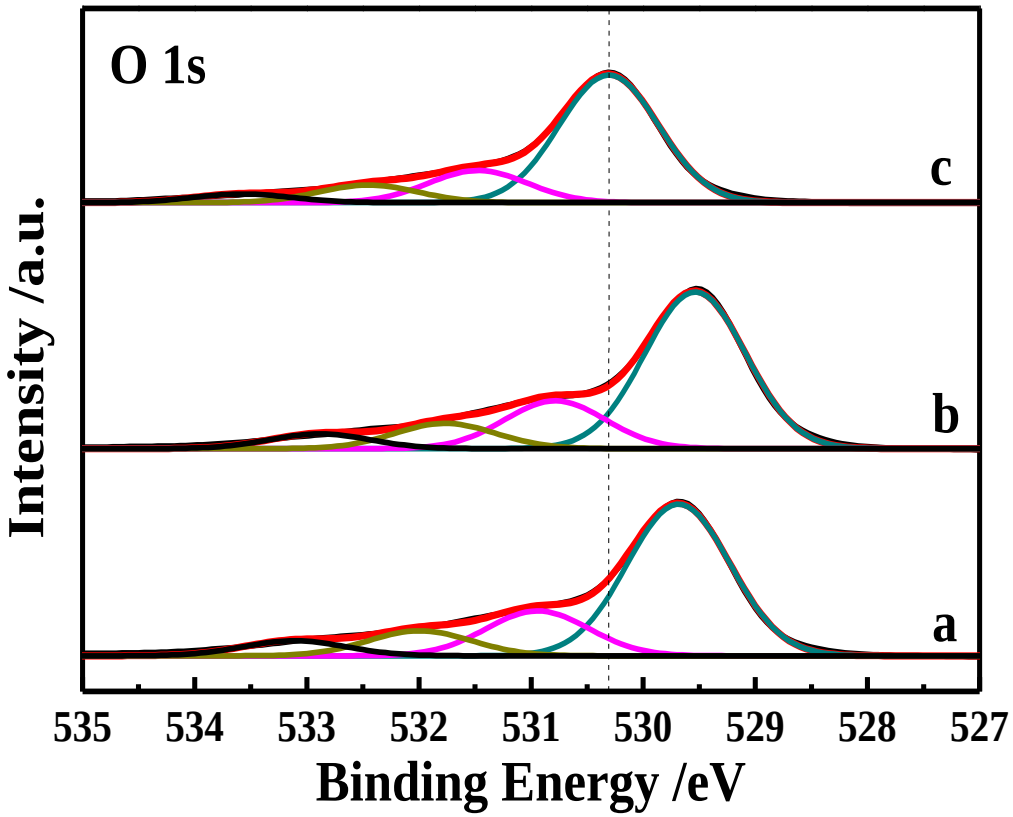

Figure 3d. C1s spectrum of XPS spectra for all prepared materials. Curve a, b and c corresponded to material a, b and c.

To further probe the chemical valences of the elements in all prepared materials, X-ray photoelectron spectroscopy (XPS) measurement was carried out and the results are displayed in the serial figures of Fig.3. The wide scan XPS survey spectra displayed in Fig. 3a effectively confirmed the existence of C, O and Co elements in all resultant materials, being in line with the EDS analysis (Fig.2c). The Co 2p XPS spectra of all prepared materials were given in Fig. 3b. For all synthesized materials, two main peaks positioned at about 780.4 eV and 795.5eV, showing a spin energy separation of about 15 eV, were displayed, which could be respectively assigned to Co $2p_{3/2}$ and Co $2p_{1/2}$ core levels of Co_3O_4 [13]. Two typical satellite peaks assigned to Co_3O_4 appearing at 786.2 eV and 804.2eV were also observed clearly in all prepared materials, indicating that Co_3O_4 as one main component was produced in all as-produced materials. The small peaks observed at 782.0 eV and 797.3 eV should be respectively ascribed to the Co^{2+} $2p_{3/2}$ and Co^{2+} $2p_{1/2}$ energy levels of CoO based on the former report [19]. Careful observation indicated that the characteristic satellite peak belonging to CoO phase was only exhibited in material a and b, which explicitly documented that more less amount of CoO was synthesized in material c. In the C 1s XPS spectra (Fig.3c), two obvious deconvoluted peaks were seen in all materials. The largest peak for material a, b and c was, respectively, centered at about 284.4, 284.3 and 284.7 eV, which was generally originated from the C=C bond [11]. Compared to material a and b, the peak position of C=C bond in material c was slightly shifted to a higher binding energy, suggesting that more amounts of cobalt oxides with higher valence were prepared in material c [27], that is to say, more amount of Co_3O_4 was fabricated in material c, agreeing well with the XRD results (Fig.2a) and Co 2p XPS spectra

(Fig.3b). The other main peak centered at 286 eV was commonly ascribed to C-O bond of the carbon particles [11]. It was clear that in material a and b, an evident and broad peak at 286.5 eV was also visible, confirming the presence of C-C bond in the synthesized materials [11]. Four deconvoluted peaks were presented in the O 1s XPS spectrum (Fig. 3d) for all prepared materials. The largest O 1s peaks assigned to the Co-O bond in Co_3O_4 [28] were observed at 529.6, 529.5 and 530.3 eV for material a, b and c, respectively. Also, relative to material a and b, the peak position of O 1s XPS spectrum for material c showed a higher energy direction shifting, further convincing that more cobalt oxides with higher valences were fabricated in material c. The O 1s peaks appearing at 530.9, 532.0 and 533.1eV were, respectively, ascribed to hydroxyl, oxygen vacancies and chemisorbed water in the light of the former report [19]. Again, the XPS results effectively demonstrated that the main component of material c was Co_3O_4, and besides carbon particles, CoO and Co_3O_4 were the other two main substances of material both a and b, being in accord with the XRD results.

3.3 Electrochemical properties

The initial charge-discharge plots recorded at 100 mA g^{-1} for all synthesized materials are displayed in Fig.4a. In the charging stage, an oblique line appearing below 1.8V was accompanied by a relatively flat line. While, in the discharge step, a flat potential terrace was displayed at about 1.2 V which was followed a sloped line. The curve shape of Fig.4a was very similar to that of Co_3O_4 [13], further assuring that the main component of all prepared materials was Co_3O_4. The initial discharge capacities at 100 mA g^{-1}, estimated from Fig.4a, of material a, b and c were 600, 612 and 878 mAh g^{-1}, respectively. Thus, the largest discharge capacity value was delivered by material c, which should be ascribed to its higher crystallinity (Fig.2a) and larger amount of cobalt oxides (Fig.2c).

The plots representing the relationship between the cycle number and the discharge capacity value are given in Fig. 4b. The discharge capacity value decreased evidently with increasing the cycle number, however, the descending degree was rather different from each other. For instance, after 20 cycles, the discharge capacities for material a, b and c studied at 100 mA g^{-1} decreased from 596 to 452 mAh g^{-1}, 610 to 454 mAh g^{-1} and 878 to 649 mAh g^{-1}, corresponding to a capacity retention of 75.8%, 74.4% and 73.8%, respectively. The discharge capacities after 20 cycles for all prepared materials were still remarkably larger than the theoretical capacities of both graphite (372 mAh g^{-1}) [29] and lithium titanate ($Li_4Ti_5O_{12}$, 175 mAh g^{-1}) [30], substantially saying that all synthesized materials could be applied as LIBs anode materials.

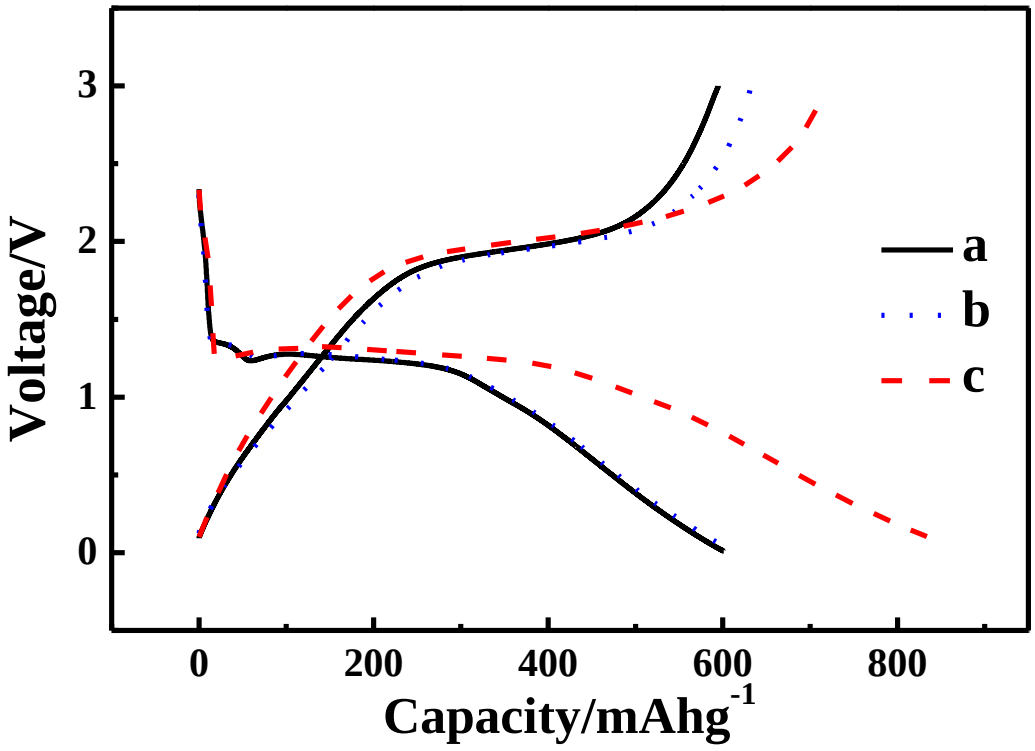

Figure 4a. The initial charge-discharge profiles for all prepared materials which were recorded at 100 mA g^{-1} in the potential limit of 0.01-3.0 V. Curve a, b and c corresponded to material a, b and c.

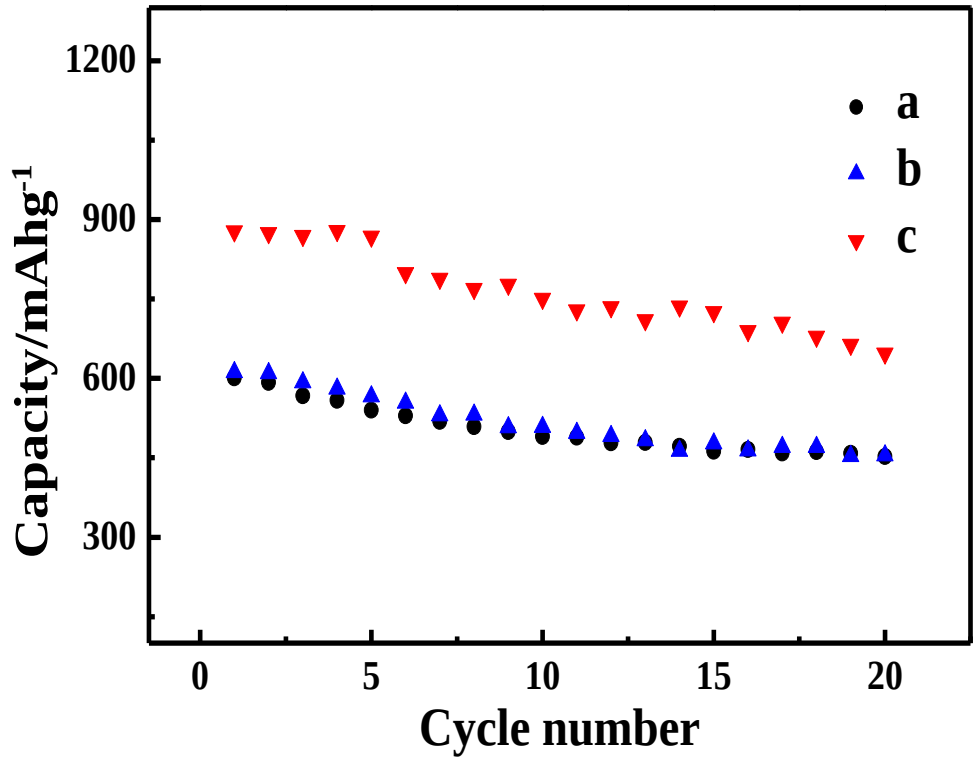

Figure 4b. Cycling performance of all resultant materials at a current density of 100 mA g^{-1}. Curve a, b and c corresponded to material a, b and c.

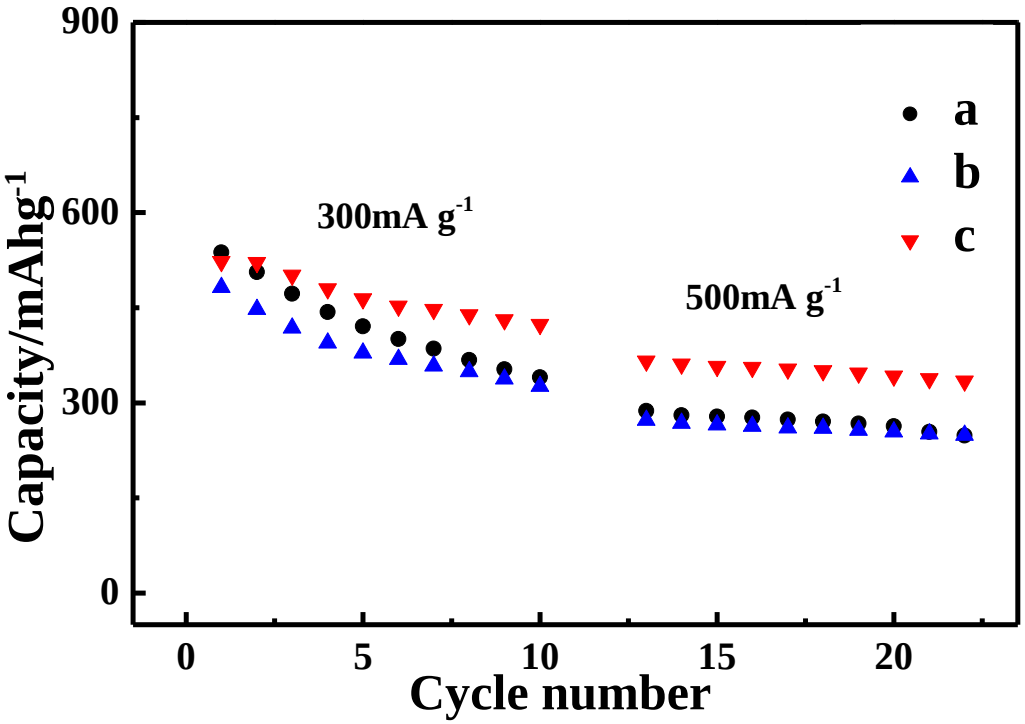

Figure 4c. Rate capabilities of all resultant samples. The current densities were 300 and 500 mA g^{-1}, respectively. In each rate test, 10 cycles were performed. Curve a, b and c corresponded to material a, b and c.

The lines describing the rate capabilities of all synthesized materials are given in Fig.4c. In all rate measurements, material c delivered the largest discharge capacity amongst all synthesized materials. For example, at 300 mA g^{-1}, the discharge capacity of material c recorded at the first cycle and the tenth cycle were 521 and 425 mAh g^{-1}, respectively, corresponding to a capacity retention value of about 81.5%. While at 500 mA g^{-1}, the discharge capacity of material c decreased from 366 mAh g^{-1} at the first cycle to 336 mAh g^{-1} at the tenth cycle, delivering a higher capacity retention value close to 91.8%. Summarily, material c exhibited the best rate capability among all prepared materials.

The CV lines noted at 1mV s^{-1} of all resultant materials are presented in Fig. 5a. As is known to all, the anodic peaks appearing in the CV curves were resulted from a delithiation process (an electrochemical oxidation reaction), and the cathodic peaks corresponded to a lithiation process (an electrochemical reduction reaction) [30]. Thus, based on the previous works, the anodic peak at about 2.0V should be assigned to the oxidation of metallic cobalt to be Co_3O_4 and the decomposition of Li_2O [11, 31], i.e., $4Li_2O + 3Co \rightarrow Co_3O_4 + 8Li^+ + 8e^-$. And the cathodic peak at around 0.8 V should be due to the electrochemical reduction of Co_3O_4 to be metallic cobalt, along with the formation of Li_2O, namely, $Co_3O_4 + 8Li^+ + 8e^- \rightarrow 4Li_2O + 3Co$. The presence of both oxidation and reduction peaks in the CV curves effectively asserted that the extraction and insertion process of lithium ions in all produced materials could proceed very well. Generally, the peak area of a CV curve was directly proportional to the amounts of electric charge transferred in an electrochemical reaction [32, 33]. Thus, material c delivered the largest amount of electric charge in the charging/discharging procedure thanks to its largest peak areas among all prepared materials, just interpreting the fact that the discharge capacity value of

material c was the largest one among all produced materials (Fig.4a, 4b and 4c).

The Nyquist plots, recorded after 20 cycles (after the experiment of Fig.4b), of all prepared materials are provided in Fig.5b. Apparently, the Nyquist plot was assembled by a semicircle existing in the region of high frequency and a sloped line emerging in the lower frequency limit, indicating that the extraction/insertion mechanism of Li^+ in all materials was similar to each other, being in agreement with the CV results (Fig.5a). As a general rule, in the EIS measurement, the semicircle of a Nyquist plot corresponded to a parallel circuit having a resistor and a capacitor, and the diameter of the semicircle was roughly equal to the value of R_{ct} (R_{ct} was called as charge transfer resistance) [32]. And usually, the larger the diameter is, the bigger is its value of R_{ct}. The R_{ct} values of material a, b and c were approximately evaluated to be 116, 132 and 95 Ω, respectively, implying that material c had the fastest intercalation/de-intercalation kinetics, supporting the fact that the largest discharge capacity value was delivered by material c.

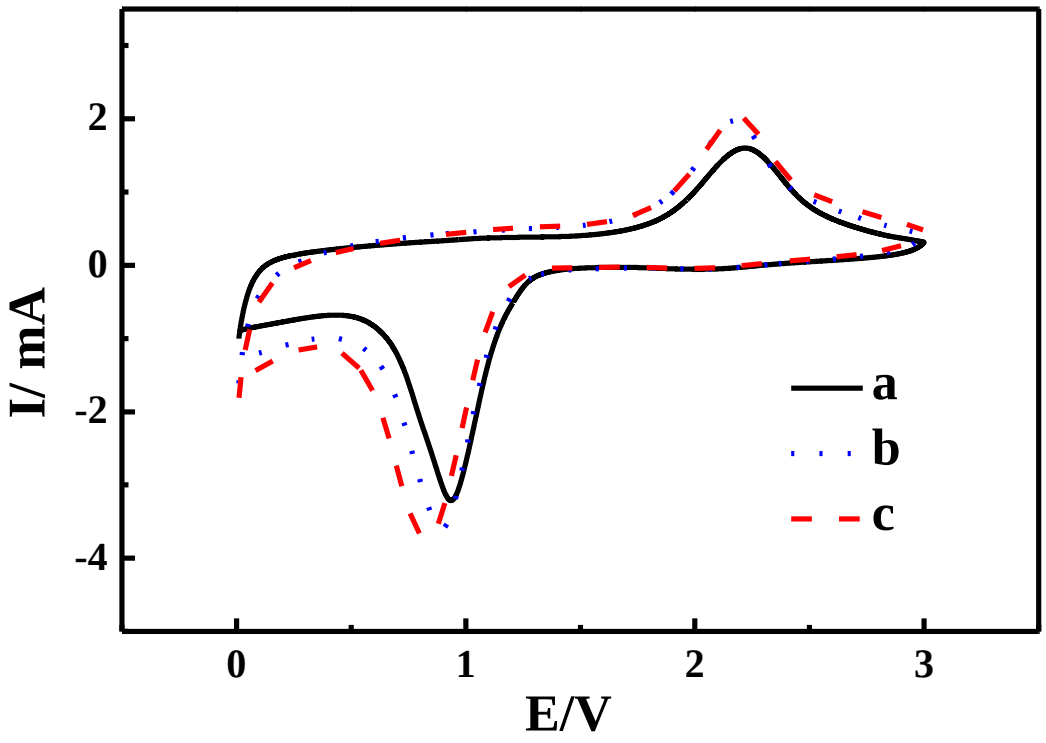

Figure 5a. Cyclic voltammetry (CV) curves at 1mV s^{-1} for all produced materials. Curve a, b and c corresponded to material a, b and c.

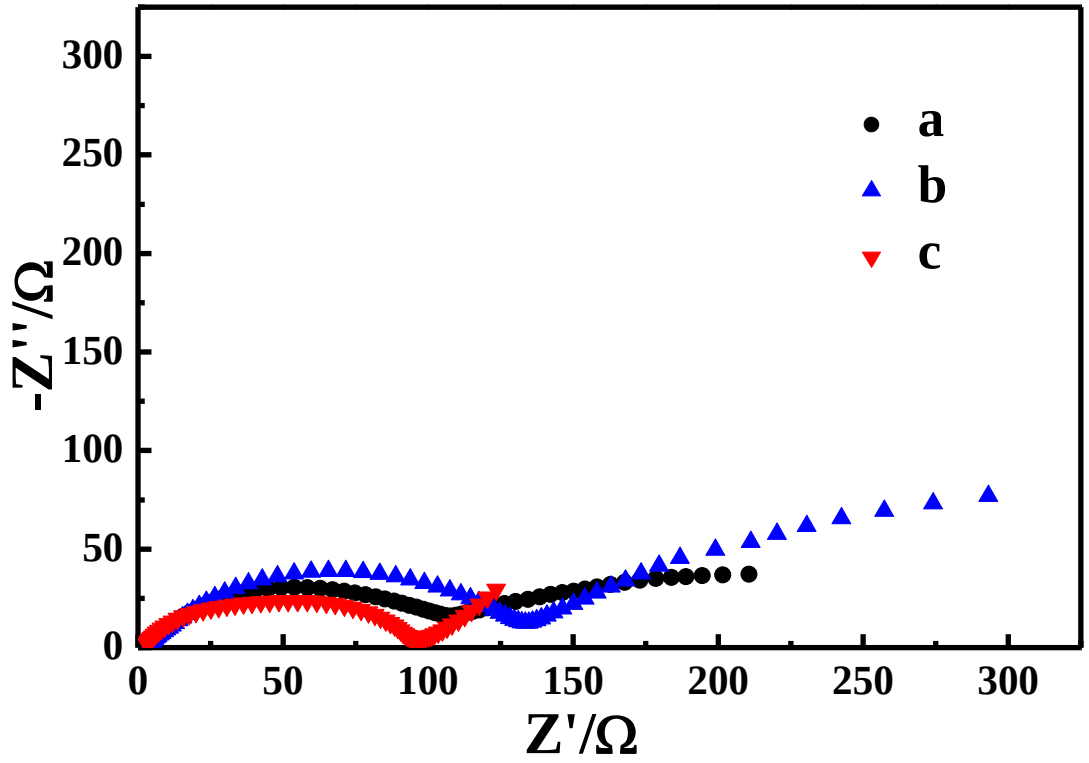

Figure 5b. Nyquist plots for all obtained materials. Curve a, b and c corresponded to material a, b and c.

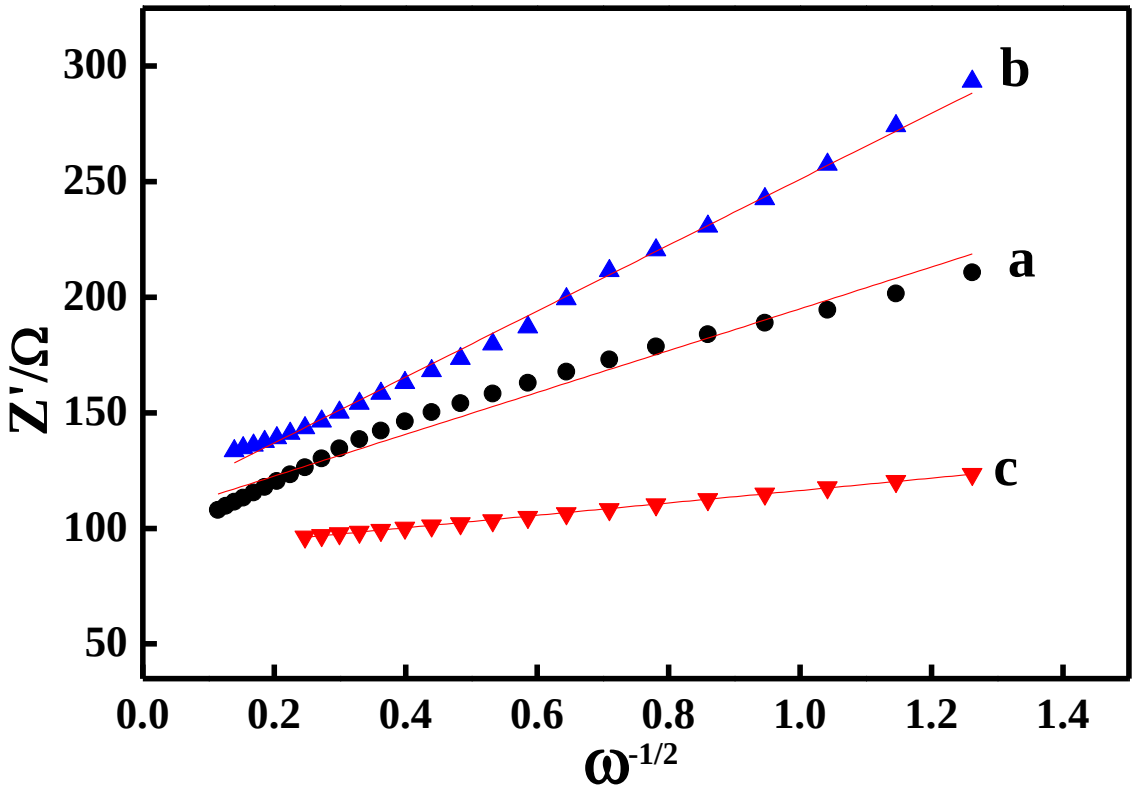

Figure 5c. Curves of between Z' and $\omega^{-1/2}$. Curve a, b and c corresponded to material a, b and c.

The lithium ion diffusion coefficient (D_{Li}), through which the diffusion rates of the lithium ions in various materials could be estimated directly, was also a key factor. To calculate the D_{Li} value, the

value of Warburg factor σ must be obtained firstly from equation (1) [34], namely,

$$Z_{re} = R_s + R_{ct} + \sigma\,\omega^{-1/2} \quad (1)$$

Z_{re} was the Z' of the Nyquist plot. The scientific meanings of R_s and R_{ct} have been explained in ref.34. ω, angular frequency, was connected with frequency (f) using $\omega=2\pi f$. Therefore, the value of σ could be easily estimated from the line showing the relationship between Z_{re} and $\omega^{-1/2}$. It was evident that material c, due to its smallest value of slope (Fig. 5c), delivered the smallest value of σ among all resultant materials. Next, the value of D_{Li} could be valued employing equation (2) [35], namely,

$$D_{Li} = \frac{(RT)^2}{2(An^2F^2C_{Li}\sigma)^2} \quad (2)$$

R, T, F and A had their common scientific meanings [35]. n was the number of electrons transferred in the lithiation/delithiation reaction, and C_{Li} was the concentration of Li^+ in an electrode material. To simplify the analysis, besides σ, the values of the parameters existing in equation (2) were supposed to be identical for all prepared materials. Thus, material c delivered the largest value of D_{Li} because of its smallest value of σ, which was well responsible for the fact that among all resultant materials material c showed the best electrochemical performance.

4. CONCLUSIONS

For the first time, octahedron particles of tricobalt tetraoxide (Co_3O_4) with a size more than 8 μm were prepared via an ionic liquid-present dissolving-drying-calcination method using cobaltous acetate tetrahydrate ($Co(CH_3COO)_2{\cdot}4H_2O$) as the starting material. In this work, three kinds of ionic liquids were, for the first time, utilized in the preparation system. XRD measurement, along with the XPS analysis, strongly revealed that Co_3O_4 was the major component of material c, and CoO as the other component was fabricated in material a and b. In particular, Co_3O_4 particles with well-defined octahedron structure and a size close to 8.3 μm were produced in material c. Most importantly, material c delivered a discharge capacity of 647 mAh g^{-1} at 100 mA g^{-1} after 20 cycles. And even at the current density of 500 mA g^{-1}, the discharge capacity of material c was higher than 336 mAh g^{-1} after 10 cycles. Developing a novel ionic liquid-present preparation system to fabricate Co_3O_4 and showing the successful preparation of micron-sized Co_3O_4 octahedron particles are the main contributions of this work, which suggested that other kinds of metal oxides with particular morphology might also be prepared via this newly developed ionic liquid-present preparation method.

ACKNOWLEDGMENTS

The work was supported by the Ministry of Science and Technology of China (No. 2019YFE010200 and 2019YFA0705703) and the National Natural Science Foundation of China (No. U1564205) and Technical Innovation Advanced Research Foundation of Hebei Normal University (L2018K03).

References

1. P. Witheya, C. Johnston and J. Guo, *Renew. Sust. Energ. Rev.*, 115 (2019) 109408.
2. I. López, E. Ibarra, A. Matallana, J. Andreu and I. Kortabarria, *Renew. Sust. Energ. Rev.*, 114 (2019) 109336.
3. Y. Liu, Z. Ge, Z. Sun, Y. Zhang, C. Dong, M. Zhang, Z. Li and Y. Chen, *Nano Energy*, 67 (2020) 104216.
4. K. Xu, L. Ma, X. Shen, Z. Ji, A. Yuan, L. Kong, G. Zhu and J. Zhu, *Electrochim. Acta*, 323 (2019) 134855.
5. K. Ding, P. Wang, J. Zhao, Y. Li, Y. Chen, Y. Zhang, B. Wei, Y. Sun and J. Pan, *Int. J. Hydrogen Energ.*, 42 (2017) 9766.
6. W. Jiang, J. Pan and X. Liu, *J. Power Sources*, 409 (2019) 13.
7. S. Osman, R. A. Senthil, J. Pan and Y. Sun, *J. Power Sources*, 414 (2019) 401.
8. H. He, W. Fu, H. Wang, H. Wang, C. Jin, H. Fan and Z. Liu, *Nano Energy*, 34 (2017) 449.
9. P. Jing, P. Wang, M. Liu, W. Gao, Y. Cui, Z. Wang and Y. Pu, *J. Alloy. Compd.*, 774 (2019) 236.
10. H. Duan, L. Du, S. Zhang, Z. Chen and S. Wu, *J. Mater. Chem. A*, 7 (2019) 8327.
11. J. Deng, X. Lv, J. Zhong and X. Sun, *Appl. Surf. Sci.*, 475 (2019) 446.
12. Y. Zhang, M. Hu, M. Yuan, G. Sun, Y. Li, K. Zhou, C. Chen, C. Nan and Y. Li, *Nano Res.*, 12 (2019) 299.
13. Y. Liu, H. Wan, N. Jiang, W. Zhang, H. Zhang, B. Chang, Q. Wang, Y. Zhang, Z. Wang, S. Luo and H. Sun, *Solid State Ionics*, 334 (2019) 117.
14. X. Xiao, X. Liu, H. Zhao, D. Chen, F. Liu, J. Xiang, Z. Hu and Y. Li, *Adv. Mater.*, 24 (2012) 5762.
15. F. Zheng and L. Wei, *J. Alloy. Compd.*, 790 (2019) 955.
16. M. Xiao, Y. Meng, C. Duan, F. Zhu and Y. Zhang, *J. Mater. Sci.- Mater. El.*, 30 (2019) 6148.
17. K. Ding, Y. zhao, L. Liu, Y. Li, L. Liu, L. Wang, X. He and Z. Guo, *Electrochim. Acta*, 176 (2015) 240.
18. F. Chen, Y. Yuan, L. Ye, M. Zhu, G. Cai, S. Yin, J. Yang and S. Guo, *Mater. Lett.*, 237 (2019) 213.
19. M. Cheng, S. Duan, H. Fan and R. Wang, *CrystEngComm*, 18 (2016) 6849.
20. K. Ding, H. Gu, C. Zheng, L. Liu, L. Liu, X. Yan and Z. Guo, *Electrochim. Acta*, 146 (2014) 585.
21. G. Xu, J. Li, L. Huang, W. Lin and S. Sun, *Nano Energy*, 2 (2013) 394.
22. Z. Jiang, C. Liu, L. Zhang, T. Wei, H. Jiang, J. Zhou, M. Shi, S. Liang, Z. Su, Z. Fan, *J. Power Sources*, 441 (2019) 227182.
23. C. Li, Y. Chen, B. Wei, K. Ding, Y. Zhang, X. Shi and J. Zhou, *Int. J. Electrochem. Sci.*, 12 (2017) 11701.
24. L. Bao, Y. He, C. Peng, Y. Li, E. Ou and W. Xu, *Mater. Lett.*, 235 (2019) 88.
25. N. Sheibani, M. Kazemipour, S. Jahani and M. M. Foroughi, *Microchem. J.*, 149 (2019) 103980.
26. K. Ding, H. Wang, B. Wei, Y. Sun, X. Shi, C. Li, H. Wang, H. Dou and J. Pan, *Mater. Chem. Phys.*, 213 (2018) 422.
27. J. B. Gieu, C. Courrèges, L. E. Ouatani, C. Tessier and H. Martinez, *J. Power Sources*, 318 (2016) 291.
28. W. Song, A. S. Poyraz, Y. Meng, Z. Ren, S. Chen and S. Sui, *Chem. Mater.*, 26 (2014) 4629.
29. H. Kim, H. Kim, S. Muhammad, J. H. Um, M. S. A. S. Shah, P. J. Yoo and W. S. Yoon, *J. Power Sources*, 446 (2020) 227321.
30. K. Ding, B. Wei, Y. Zhang, C. Li, X. Shi and J. Pan, *Int. J. Electrochem. Sci.*, 12 (2017) 8381.
31. N. Jayaprakash, W. D. Jones, S. S. Moganty and L. A. Archer, *J. Power Sources*, 200 (2012) 53.
32. K. Ding, J. Han, X. Gao, L. Zhou and R. Qu, *Mater. Chem. Phys.*, 232 (2019) 354.
33. L. Zhang, Y. Ouyang, S. Wang, Y. Gong, M. Jiang, W. Yuan and C. Li, *J. Power Sources*, 447 (2020) 227248.
34. M. Krajewski, M. Michalska, B. Hamankiewicz, D. Ziolkowska, K. P. Korona, J. B. Jasinski, M.

Kaminska, L. Lipinska and A. Czerwinski, *J. Power Sources*, 245 (2014) 764.
35. T. Yi, H. Liu, Y. Zhu, L. Jiang, Y. Xie and R. Zhu, *J. Power Sources*, 215 (2012) 258.